Effect of ion migration on the self-assembly of porous nanostructures in anodic oxides

L. G. Stanton and A. A. Golovin
Department of Engineering Sciences and Applied Mathematics, Northwestern University, 2145 Sheridan Road, Evanston, IL 60208 USA
(Received 7 July 2008; published 22 January 2009)

The self-organization of porous nanostructures in anodic oxide is considered. A mathematical model which incorporates the electrochemical transport of oxygen ions within the oxide layer and the chemical reactions at the metal-oxide and oxide-electrolyte interfaces is developed. It is shown through linear stability analysis that a short-wave instability exists in certain parameter ranges which can lead to the formation of hexagonally ordered pores observed in anodized aluminum oxide. Numerical simulations validate these results.

DOI: 10.1103/PhysRevB.79.035414 PACS number(s): 82.45.Yz, 82.45.Cc, 81.05.Rm

I. INTRODUCTION

During the process of anodizing many metals in acidic electrolytes, the natural oxide layer on the anode surface grows to form a uniformly thick barrier layer. In certain metals however (e.g., aluminum,[1,2] titanium,[3–5] tin,[6] etc.), the oxide surface can become unstable and form deep pores. In particular, aluminum also has parameter regimes in which these pores self-assemble in a highly ordered hexagonal array.[7–10] As aluminum oxide can exhibit barrier layer structures as well as both regular and irregular porous arrays, we will only be considering anodized aluminum oxide (AAO) in this work, although the analysis can be easily generalized to other anode materials.

AAO has vast industrial and scientific applications. It has been used to improve the corrosion resistance, hardness, lubrication, and adhesion properties of aluminum surfaces as well as to allow for dying.[11,12] More recently, porous AAO has been used as a template for the fabrication of nanoscale particles, wires, and tubes, as pores with diameters on the order of 10 nm can be achieved.[13–16] Experimental efforts have also been able to significantly refine the regularity of the pore arrays.[17]

Theoretical attempts to understand the various phenomena and mechanisms within this system have unfortunately not been able to keep up with the quickly growing experimental progress. Although advances have been made in general aspects of AAO formation, they lack in a precise description of the physical and chemical phenomena. Models for the steady growth of a single pore were proposed in Refs. 18 and 19 and long-wave linear stability analysis was performed on a similar model in Ref. 20. Works such as in Refs. 20–22, however, lack any physical mechanism to damp short-wave disturbances. In Ref. 23 the contribution of the Laplace pressure to the activation energy of reactions at each deformable interface was proposed as a mechanism to provide this short-wave cutoff. In Ref. 24 the effects of interfacial diffusion at the metal-oxide (MO) interface were investigated, and in Ref. 25 the effects of a field-dependent oxide conductivity were explored. The model proposed by Singh *et al.*[26,27] included the contributions of elastic stress to the surface activation energies, and the validity of this model was explored experimentally in Refs. 28–31. It was shown in Refs. 26 and 27 that elastic effects can result in a short-wave instability which can explain the formation of hexagonally ordered pores.

In this work, we propose a model which incorporates the electrochemical transport of oxygen ions through the oxide layer. We use the Nernst-Planck equation to determine the flux of ions within the oxide and the Butler-Volmer relations to determine this flux at the interfaces. Once our model is established, we perform linear stability analysis on a basic state of the system to predict the onset of pattern formation at the interfaces. We show that the electromigration of ions in the oxide layer can result in a short-wave instability even in the absence of elastic effects thus leading to the formation of hexagonally ordered pore arrays. We then perform numerical simulations of the system to verify our predictions.

II. MATHEMATICAL MODEL

Consider an oxide layer on a metal surface during anodization. The domain is defined by setting the z axis to be perpendicular to the initially planar anode surface and pointing into the electrolyte. The MO and oxide-electrolyte (OE) interfaces are defined as $z=h_1(\mathbf{x},t)$ and $z=h_2(\mathbf{x},t)$, respectively, with $\mathbf{x}=(x,y)$, as shown in Fig. 1. Within the oxide, ionic flows are induced by sufficiently large electric fields.[32] Although there are several ion species present,[18] we will be considering the electrochemical transport of oxygen ions, as they are responsible for the creation of the oxide at the MO interface and result from the oxide dissolution at the OE interface.[33] In analyzing the evolution of the oxygen ion concentration $\mathcal{C}$, we assume that all chemical reactions occur at the interfaces and thus write a conservation law

$$\frac{\partial \mathcal{C}}{\partial t} + \nabla \cdot \mathbf{j} = 0, \tag{1}$$

where we are using the Nernst-Planck equation

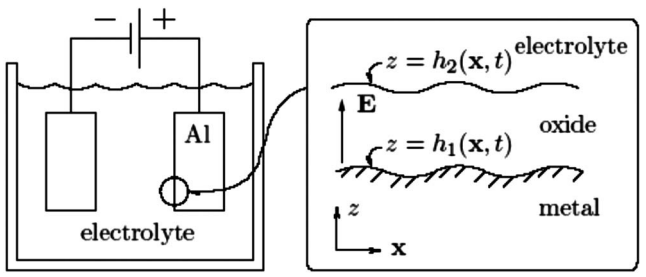

FIG. 1. Schematic of interfaces at anode surface. Note that the domain has been rotated.

$$\mathbf{j} = -\mathcal{D}\nabla\mathcal{C} - \mu\mathcal{C}\mathbf{E} \tag{2}$$

to describe the ion flux in the oxide. Here, $\mathcal{D}$ is the diffusivity, μ is the electric mobility, $\mathbf{E}$ is the electric field induced by the voltage applied to the anode, and the sign of the advection term has been taken such that $\mu > 0$. The oxide can support electric fields of the order $|\mathbf{E}| \sim 10^9$ V/m (Chap. 6 in Ref. 11), and as the magnitude of this field is very large, we neglect any perturbations to the field due to the presence of unpaired free charges and assume that the field is instead determined by the boundary conditions. If we additionally assume the oxide electric permittivity to be constant, the electric field can be modeled using Gauss' law in the form $\nabla\cdot\mathbf{E}=0$. In expressing the field in terms of its potential $\mathbf{E}=-\nabla\varphi$, we can write the bulk equations within the oxide as

$$\frac{\partial\mathcal{C}}{\partial t} = \mathcal{D}\nabla^2\mathcal{C} - \mu\nabla\varphi\cdot\nabla\mathcal{C}, \quad \nabla^2\varphi = 0. \tag{3}$$

For simplicity, we will neglect any penetration of the field into the electrolyte and assume the entire potential drop to occur within the oxide layer. This gives the Dirichlet boundary conditions

$$\varphi = V \text{ on } z = h_1(\mathbf{x},t), \quad \varphi = 0 \text{ on } z = h_2(\mathbf{x},t), \tag{4}$$

where V is the voltage applied to the anode. In the case of aluminum oxide, the total dissolution-oxidation reaction is given by $Al_2O_3 \rightleftharpoons 2Al^{3+}+3O^{2-}$. To model the ion flux at each interface, we consider only the leading-order oxidation and dissolution reactions at the MO and OE interfaces, respectively, and neglect any inverse reactions. Thus, the dissolution reaction $Al_2O_3 \rightarrow 2Al^{3+}+3O^{2-}$ takes place at the OE interface, and the oxidation reaction $2Al^{3+}+3O^{2-} \rightarrow Al_2O_3$ occurs at the MO interface. This gives the relations

$$j_n = -K_1\mathcal{C} \text{ on } z = h_1(\mathbf{x},t), \quad j_n = -K_2 \text{ on } z = h_2(\mathbf{x},t), \tag{5}$$

where the subscript n denotes the normal component of the flux $\mathbf{j}$ and the rates $K_{1,2}$ are kinetic coefficients characterizing the ionic currents produced by the reactions at each interface. We have taken the unit normal pointing away from the metal substrate at the MO interface and into the electrolyte at the OE interface. Since the dissolution reaction occurs only in the presence of the electrolyte through several intermediate reactions, in which hydrogen ions participate, we consider the rate K_2 to be proportional to the concentration of hydrogen ions, which we have assumed to be constant along the OE interface. From transition-state theory, it is also known that the reaction rates depend exponentially on the activation energies $E^a_{1,2}$ at $h_{1,2}(\mathbf{x},t)$, so we must take into account the contributions from both the electric field and the interfacial deformations (Laplace pressure) to these energies.[23,34] We then can write these rates in the form of the Butler-Volmer relations

$$K_{1,2} = k_{1,2}\exp(\alpha E_n - \gamma_{1,2}\kappa), \tag{6}$$

where $k_{1,2}$ are the reaction-rate constants in the absence of the electric field and any interfacial deformations and E_n denotes the normal component of the electric field. The parameter $\alpha = q_c\lambda_s/2k_BT$, where q_c is the absolute charge of an oxygen ion, λ_s is the thickness of the Stern layer,[35,36] and k_BT is the thermal energy (k_B is the Boltzmann constant and T is absolute temperature). Note that the symmetry factor in α has been taken as 1/2 for simplicity. This factor has been observed to be very close to 1/2 in many systems.[37] The constants $\gamma_{1,2} = \Gamma^a_{1,2}/\rho_{ox}k_BT$ for $h_{1,2}(\mathbf{x},t)$, where ρ_{ox} is the number density of the oxide, the activation surface energies $\Gamma^a_{1,2} = \rho_{ox}(\partial E^a_{1,2}/\partial\kappa)$, and $\kappa \equiv -\nabla\cdot\mathbf{n}$ is twice the mean interfacial curvature. We can finally describe the interfacial evolution by noting that the creation or dissolution of the oxide at each interface will be, respectively, proportional to the absorption or creation of oxygen ions at these interfaces. We then write

$$j_n = \rho v_n = \frac{\rho\partial_t h_{1,2}}{\sqrt{1+|\nabla h_{1,2}|^2}} \text{ on } z = h_{1,2}(\mathbf{x},t), \tag{7}$$

where v_n is the normal velocity of the interface. Using the stoichiometry of the total reaction given above, we take $\rho = 3\rho_{ox}$.

A. Nondimensional problem

We nondimensionalize the system by introducing the following transformations:

$$\{x,y,z\} \rightarrow \left(\frac{\lambda_s}{2}\right)\{x,y,z\}, \quad t \rightarrow \left(\frac{\lambda_s^2}{4\mathcal{D}}\right)t,$$

$$\varphi \rightarrow \left(\frac{k_BT}{q_c}\right)\varphi, \quad \mathcal{C} \rightarrow \rho\mathcal{C}, \tag{8}$$

and by defining

$$V^* = \frac{q_cV}{k_BT}, \quad \gamma^*_{1,2} = \frac{q_c\gamma_{1,2}}{\alpha k_BT}, \quad k^*_1 = \frac{\alpha k_1}{\mu}, \quad k^*_2 = \frac{\alpha k_2}{\rho\mu}. \tag{9}$$

Note that we have used the Einstein mobility relation $\mu = q_c\mathcal{D}/k_BT$ to simplify some of these quantities. This reduces our system to

$$\frac{\partial\mathcal{C}}{\partial t} = \nabla^2\mathcal{C} - \nabla\varphi\cdot\nabla\mathcal{C}, \quad \nabla^2\varphi = 0 \text{ for } z \in (h_1,h_2), \tag{10}$$

$$\varphi = V^*, \quad \frac{\partial\mathcal{C}}{\partial n} - \frac{\partial\varphi}{\partial n}\mathcal{C} = k^*_1\mathcal{C}\exp\left(\gamma^*_1\nabla\cdot\mathbf{n} - \frac{\partial\varphi}{\partial n}\right) = -v_n \text{ on } z = h_1(\mathbf{x},t), \tag{11}$$

$$\varphi = 0, \quad \frac{\partial\mathcal{C}}{\partial n} - \frac{\partial\varphi}{\partial n}\mathcal{C} = k^*_2\exp\left(\gamma^*_2\nabla\cdot\mathbf{n} - \frac{\partial\varphi}{\partial n}\right) = -v_n \text{ on } z = h_2(\mathbf{x},t). \tag{12}$$

For the remainder of the analysis, we will drop the asterisks for convenience.

B. Basic state

We begin our analysis of the system (10)–(12) by seeking a traveling-wave solution corresponding to two planar inter-

faces with a fixed distance L between them moving with speed $v>0$ in the $-z$ direction. This would represent a barrier layer in which the oxidation of the metal substrate is balanced by the dissolution of the oxide into the electrolyte. Go over to the moving reference frame $\zeta=z+vt$ with the (x,y) plane coincident with the MO interface, and let $\varphi=\varphi_0(\zeta)$ and $\mathcal{C}=\mathcal{C}_0(\zeta)$. Then Eq. (10) becomes

$$\mathcal{C}_0'' - (v + \varphi_0')\mathcal{C}_0' = 0, \quad \varphi_0'' = 0, \tag{13}$$

where primes denote differentiation with respect to ζ. The potential can be expressed in terms of the oxide thickness $L=h_2-h_1$ as

$$\varphi_0(z) = V - E\zeta, \quad E = V/L. \tag{14}$$

The boundary conditions (11) and (12) are reduced to

$$v = k_1\mathcal{C}_0 e^E, \quad \mathcal{C}_0' + (E - k_1 e^E)\mathcal{C}_0 = 0 \ \text{ at } \ z = 0, \tag{15}$$

$$v = k_2 e^E, \quad \mathcal{C}_0' + E\mathcal{C}_0 = k_2 e^E \ \text{ at } \ z = L. \tag{16}$$

This gives the system velocity and concentration as

$$v = \frac{k_2}{k_1}E, \quad \mathcal{C}_0 = \frac{k_2}{k_1}, \tag{17}$$

where the nondimensional electric field is defined as a solution of the transcendental equation

$$E = k_1 \exp(E). \tag{18}$$

Although this equation is valid for all values of E, this basic state exists only for $k_1 \leq 1/e$. In this case, there are two solutions which correspond to two different oxide thicknesses, and it can be shown that the basic state corresponding to the thicker oxide layer will never be unstable with respect to spatially homogeneous perturbations. From now on, we shall hence only consider this basic state. For the advection speed of ions to exceed the speed of the reference frame, we must have $E>v$ which is satisfied if $k_1>k_2$. Note that this basic state is invariant with respect to the length L as long as the field E is kept fixed. In other words, the barrier layer thickness scales linearly with the voltage, which has been observed experimentally (Chap. 6 in Ref. 11).

III. LINEAR STABILITY ANALYSIS

We next examine the stability of this basic state solution by perturbing the electric potential, ion concentration, and interfaces as

$$\varphi = V - E\zeta + \hat{\varphi}(\zeta)e^{\sigma t + i\mathbf{q}\cdot\mathbf{x}}, \quad \mathcal{C} = \frac{k_2}{k_1} + \hat{\mathcal{C}}(\zeta)e^{\sigma t + i\mathbf{q}\cdot\mathbf{x}}, \tag{19}$$

$$h_1 = \hat{h}_1 e^{\sigma t + i\mathbf{q}\cdot\mathbf{x}}, \quad h_2 = L + \hat{h}_2 e^{\sigma t + i\mathbf{q}\cdot\mathbf{x}}, \tag{20}$$

where $\mathbf{q}$ is the wave vector of a given normal mode and σ is the growth rate of that mode. We then linearize to obtain the following problems:

$$\hat{\mathcal{C}}'' + (E - v)\hat{\mathcal{C}}' - (\sigma + q^2)\hat{\mathcal{C}} = 0, \quad \hat{\varphi}'' - q^2\hat{\varphi} = 0, \tag{21}$$

where $q=|\mathbf{q}|$. Using the linearized boundary conditions

$$\hat{\varphi}(0) = -\varphi_0'\hat{h}_1 = E\hat{h}_1, \quad \hat{\varphi}(L) = -\varphi_0'\hat{h}_2 = E\hat{h}_2, \tag{22}$$

the solution to the potential perturbation eigenfunction is

$$\hat{\varphi}(\zeta) = -E\frac{\sinh[q(\zeta - L)]}{\sinh(qL)}\hat{h}_1 + E\frac{\sinh(q\zeta)}{\sinh(qL)}\hat{h}_2. \tag{23}$$

The remaining linearized boundary conditions are

$$\hat{\mathcal{C}}'(0) = (1 - E)\mathcal{C}_0\hat{\varphi}'(0) + \gamma_1 E\mathcal{C}_0 q^2\hat{h}_1, \tag{24}$$

$$E\hat{\mathcal{C}}(0) = E\mathcal{C}_0\hat{\varphi}'(0) - (\sigma + E\gamma_1 q^2\mathcal{C}_0)\hat{h}_1 \tag{25}$$

at the MO interface ($\zeta=0$) and

$$\hat{\mathcal{C}}'(L) + E\hat{\mathcal{C}}(L) = (\mathcal{C}_0 - k_2 e^E)\hat{\varphi}'(L) + \gamma_2 k_2 e^E q^2\hat{h}_2, \tag{26}$$

$$0 = -k_2 e^E\hat{\varphi}'(L) + (\sigma + \gamma_2 k_2 e^E q^2)\hat{h}_2 \tag{27}$$

at the OE interface ($\zeta=L$). The general solution to the concentration perturbation eigenfunction is given by

$$\hat{\mathcal{C}}(\zeta) = c_1 e^{\lambda^+\zeta} + c_2 e^{\lambda^-\zeta}, \quad \lambda^{\pm} = -\frac{1}{2}(E - v) \pm \frac{1}{2}\sqrt{(E - v)^2 + 4(\sigma + q^2)}. \tag{28}$$

We can see from this system that the vector of interfacial perturbation eigenfunctions, $\mathbf{h}=(\hat{h}_1,\hat{h}_2)$, can be written as

$$\mathbf{h}(\sigma,q) \sim \left[\cosh(qL) - \left(\frac{k_1\sigma + \gamma_2 k_2 E q^2}{k_2 E^2 q}\right)\sinh(qL), 1\right]. \tag{29}$$

We should expect $|\hat{h}_1|<|\hat{h}_2|$, as the unsaturated pore growth occurs at the OE interface. Furthermore, we expect these components to be of the same sign to imply a sinuous mode (as opposed to a varicose mode). This gives the relations

$$0 < \cosh(qL) - \left(\frac{k_1\sigma + \gamma_2 k_2 E q^2}{k_2 E^2 q}\right)\sinh(qL) < 1 \tag{30}$$

and allows us to neglect regions of parameter space which lead to unphysical results. We next write the boundary conditions (24)–(26) as the system $\mathbf{\Lambda u}=\mathbf{0}$, where the vector of unknowns $\mathbf{u}=(c_1,c_2,\hat{h}_1,\hat{h}_2)$. For $\mathbf{u}$ to have a nontrivial solution, the linear operator must be singular, and hence we set $\det(\mathbf{\Lambda})=0$ to determine the dispersion relation. This yields a quite cumbersome implicitly defined function $\sigma(q)$, which can be handled numerically. We can now use this relation to determine the stability of the basic state and find parameter regimes in which the system yields a short-wave instability, which is necessary for the initial development of ordered pores. It is also known that systems which lack reflectional symmetry near the onset of such an instability will then support quadratic resonances of perturbations and lead to hexagonal spatial patterns.[38,39] As the applied electric field breaks this symmetry, we can then expect hexagonally ordered pores to develop at the interfaces in these regimes. Parameter regimes in which long-wave instabilities are ob-

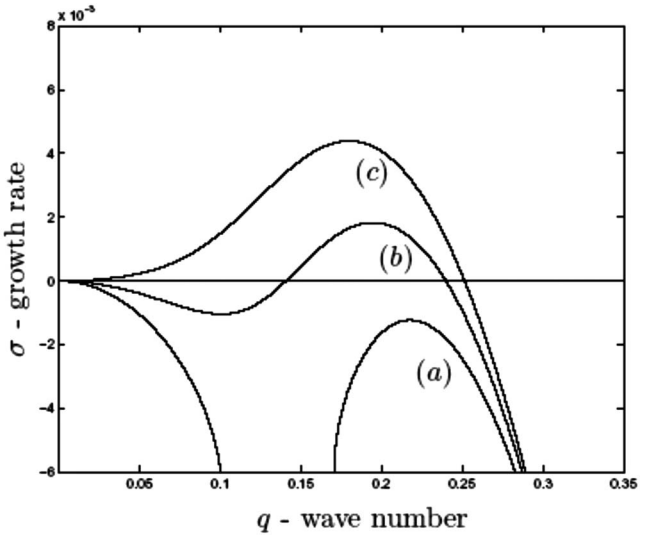

FIG. 2. Dependence of the dispersion curves on the rescaled voltage V: (a) $V=3.8$, (b) $V=4$, and (c) $V=4.2$. The remaining parameters are $k_1=0.35$, $k_2=0.21$, $\gamma_1=5.25$, and $\gamma_2=2.9$.

served would correspond to the development of irregular pores as seen in anodized titanium oxide for example or in AAO for some electrolytes.[10] Plots of $\sigma(q)$ are shown in Figs. 2 and 3 as the laboratory control parameters V and pH are varied respectively. In Fig. 2, we see that the instability grows from short-wave (curve b) to long-wave (curve c) with an increase in the applied voltage. Additionally, there is also a decrease in the maximal excited wave number, which corresponds to an increase in the pore diameter and spacing as seen in experiment.[10,18,40] Figure 3 shows the dependence of the dispersion curves on the pH of the electrolyte. As the parameter k_2 is linearly dependent on the concentration of hydrogen ions, the pH will then logarithmically depend on the inverse of k_2. It is seen that an increase in pH (or decrease in k_2) has qualitatively similar effects as those of increases in the voltage. This has also been observed experimentally.[18,20] We can also use this dispersion relation to calculate phase diagrams as shown in Fig. 4 to determine parameter regimes for damped short-wave and long-wave instabilities. The boundaries of these instability types are determined from the system

$$\sigma = 0, \quad \frac{\partial \sigma}{\partial q} = 0. \tag{31}$$

The phase diagram in the applied voltage and electrolyte pH would suggest that, at higher voltages, a lower pH would be required to obtain a short-wave instability. The second phase diagram in the interfacial reaction rates shows that there is only a very small range in which physically valid short-wave instabilities are observed. This narrow domain of chemical kinetic coefficients might explain why the self-assembly of ordered pores is only observed for aluminum and not other substrate materials characterized by different chemical reactions.

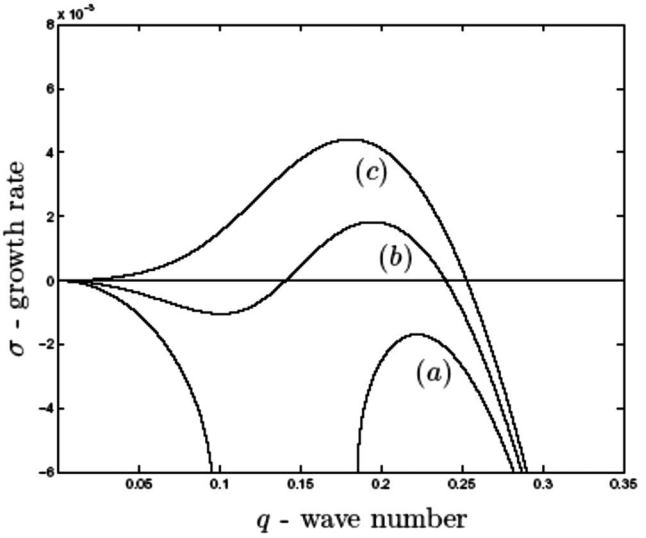

FIG. 3. Dependence of dispersion curves on pH which increases logarithmically as k_2 decreases: (a) $k_2=0.215$, (b) $k_2=0.210$, and (c) $k_2=0.205$. The remaining parameters are $V=4$, $k_1=0.35$, $\gamma_1=5.25$, and $\gamma_2=2.9$.

IV. NUMERICAL SIMULATIONS

In performing numerical simulations of the system (10)–(12), the presence of the free interfaces can introduce some serious computational difficulties. To circumvent this issue, we transform the z coordinate as

$$z \to \frac{z - h_1(\mathbf{x},t)}{h_2(\mathbf{x},t) - h_1(\mathbf{x},t)}$$

which, although complicating the differential operators, maps the time-dependent computational domain to the fixed domain $\mathbf{x} \in \mathbb{R}^2, z \in [0,1]$. We use an explicit finite-difference method for temporal updating and spatial discretization, and periodic boundary conditions in the x and y directions are used to approximate the laterally infinite domains. To improve the accuracy without seriously affecting computational cost, we use finer meshes for the MO and OE interfaces and interpolate the fields at these interfaces with cubic splines. The numerical reference frame is also kept coincident with the MO interface to reduce round-off error, and the electric potential is calculated at each time step with successive overrelaxation iterations. A typical simulation of the two interfaces is shown in Fig. 5, where the darker areas in each figure indicate the deeper interfacial regions. The parameters were taken such that the system had a long-wave instability and the disordered array of pores can be seen. Beyond this point in the computational evolution, the deeper pores continue their unsaturated growth until numerical blowup, where the numerical approximations break down and fail to describe the system dynamics. At lower voltages, the system will be close to the onset of a short-wave instability. The results of a simulation in this parameter regime are shown in Fig. 6 in comparison to an experimental scanning electron microscopy (SEM) micrograph of AAO obtained in Ref. 17. The initial formation of hexagonal patterns with some defects can be seen, where these defects are similar to those observed experimentally in the anodization of aluminum

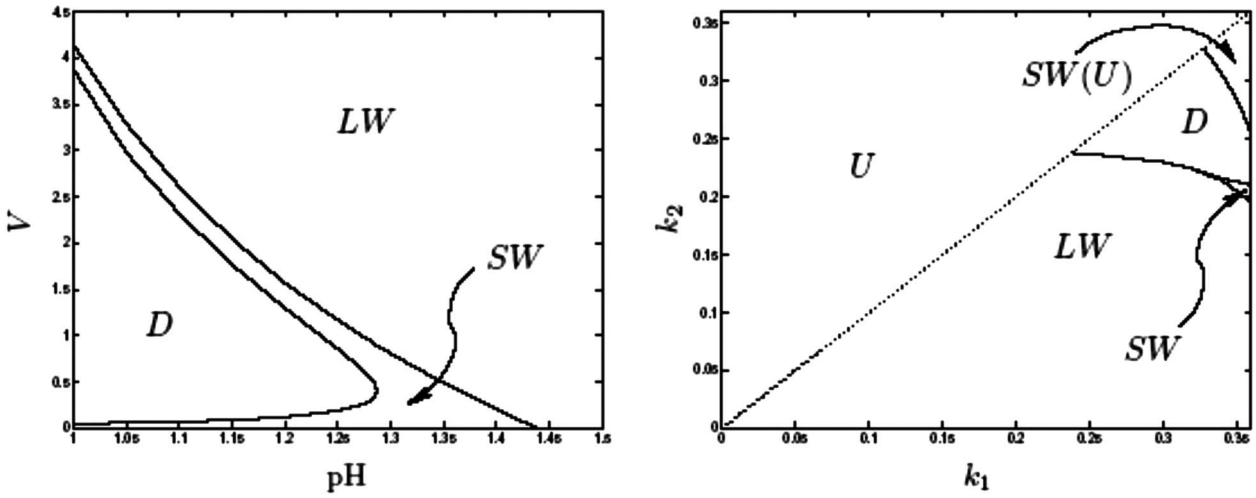

FIG. 4. Left: phase diagram in the applied voltage and pH showing regions of damped (D), short-wave (SW), and long-wave (LW) instabilities. The remaining parameters are $k_1=0.35$, $\gamma_1=5.25$, and $\gamma_2=2.9$ with $k_2=2.1$ for pH=0. Right: Phase diagram in the interfacial reaction rates. U marks the region of unphysical solutions which violate the relations $0<k_2<k_1\leq 1/e$, while SW(U) denote unphysical short-wave instabilities which violate relation (30). The remaining parameters are $V=4$, $\gamma_1=5.25$, and $\gamma_2=2.9$.

without a pretextured surface.[9] The pore diameters have also decreased with the voltage as predicted by both the linear stability analysis and experiment.[10,18,40] We note that the nondimensional length scales shown in Figs. 5 and 6 have the same order of magnitude as dimensional scales expressed in nanometers.

A more extensive numerical investigation might also yield results in which the hexagonal patterns are more ordered. There are also parameter regimes in which the growth saturates and produces an ordered array of circular depressions similar to those seen in Fig. 6. This phenomenon has been observed experimentally in works such as in Ref. 41, where single-crystal silicon is anodized in a fluoride electrolyte of neutral pH. While this is promising in supporting the generality of the mathematical model presented, this work also suggests that, in addition to the oxidation and dissolution reactions, oxygen evolution from water splitting in the electrolyte could be essential for pattern formation as an aid to pore nucleation. A more complete model which took into account the electrochemical dynamics of the electrolyte would be necessary to capture this feature.

V. CONCLUSION

A model for the initial pattern selection and development in porous AAO has been formulated. This model incorpo-

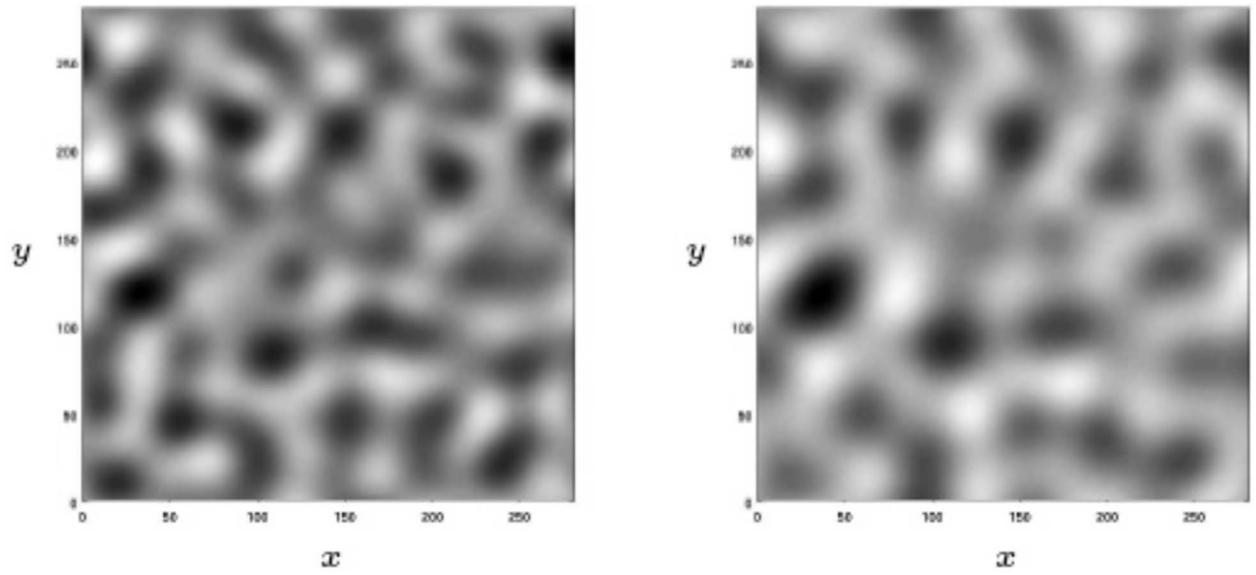

FIG. 5. Left: top-down view of OE interface. Right: top-down view of MO interface. Simulations were generated with the nondimensional parameters $V=14$, $k_1=0.36$, $k_2=0.21$, $\gamma_1=5.15$, and $\gamma_2=3.15$.

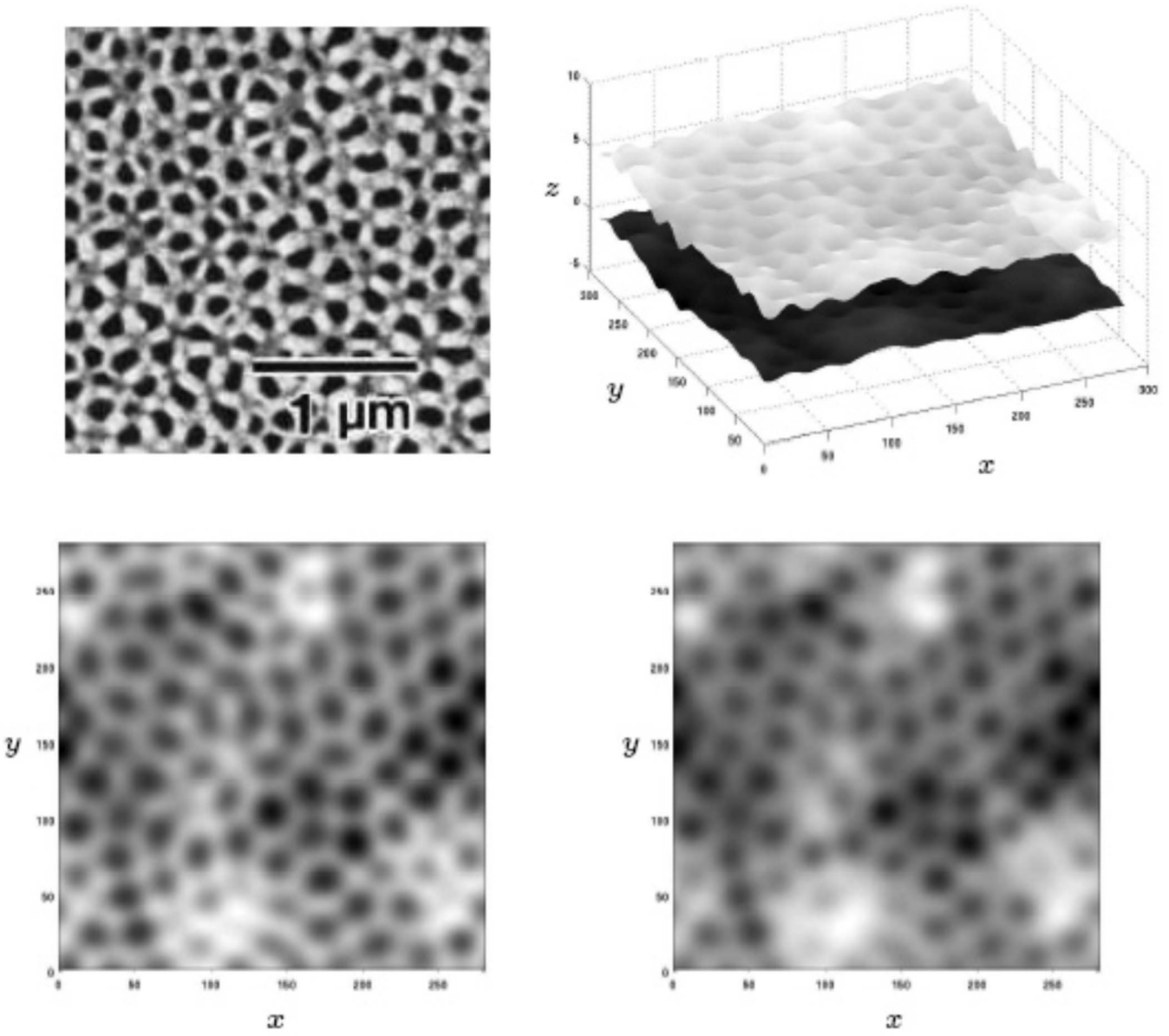

FIG. 6. Top left: SEM image of AAO hole configuration. Reprinted in part from Ref. 17 with permission of The Electrochemical Society (2001)©. Top right: numerical simulation of MO (*above in translucent image*) and OE (*below in solid image*) interfaces. Bottom left: Top down view of OE interface. Bottom right: Top down view of MO interface. Simulations were generated with the nondimensional parameters $V=4.3$, $k_1=0.36$, $k_2=0.21$, $\gamma_1=5.15$, and $\gamma_2=3.15$.

rates the electrochemical transport of oxygen ions through aluminum oxide induced by an applied electric field. We use the Nernst-Planck equation to describe the ion migration within the bulk of the oxide and use the Butler-Volmer relations to model the dependence of the interfacial reactions on activation energies, which include contributions from the electric field and surface energy. From this model, we have calculated a basic state which represents a uniformly thick barrier layer in which the rate of corrosion into the anode is balanced by the dissolution rate into the electrolyte. We have performed a linear stability analysis on this state and shown parameter regimes that produce a short-wave instability, which is necessary for the development of hexagonally ordered pore arrays. Additionally, numerical simulations of the governing equations were performed to verify the results of the linear stability analysis, and we observed the initial development of hexagonally ordered porous arrays with defects before the unsaturated growth of the pores led to numerical blowup. We can therefore conclude that ion migration through the oxide layer coupled to the nonlinear reaction rates at the two interfaces can result in a short-wave instability and the formation of hexagonally ordered pores even in the absence of the elastic effects considered in Refs. 26 and 27.

ACKNOWLEDGMENTS

This work was supported by the U.S. NSF RTG Grant No. DMS-0636574.

[1] J. P. O'Sullivan and G. C. Wood, Proc. R. Soc. London, Ser. A **317**, 511 (1970).
[2] G. E. Thompson, Thin Solid Films **297**, 192 (1997).
[3] R. Beranek, H. Hildebrand, and P. Schmuki, Electrochem. Solid-State Lett. **6**, B12 (2003).
[4] D. Gong, C. A. Grimes, O. K. Varghese, W. C. Hu, R. S. Singh, Z. Chen, and E. C. Dickey, J. Mater. Res. **16**, 3331 (2001).
[5] J. M. Macak, H. Tsuchiya, and P. Schmuki, Angew. Chem., Int. Ed. **44**, 2100 (2005).
[6] H. C. Shin, J. Dong, and M. L. Liu, Adv. Mater. (Weinheim, Ger.) **16**, 237 (2004).
[7] H. Masuda and K. Fukuda, Science **268**, 1466 (1995).
[8] H. Masuda, H. Yamada, M. Satoh, H. Asoh, M. Nakao, and T. Tamamura, Appl. Phys. Lett. **71**, 2770 (1997).
[9] A. P. Li, F. Muller, A. Birner, K. Nielsch, and U. Gosale, J. Appl. Phys. **84**, 6023 (1998).
[10] F. Y. Li, L. Zhang, and R. M. Metzger, Chem. Mater. **10**, 2470 (1998).
[11] S. Wernick, R. Pinner, and P. G. Sheasby, *The Surface Treatment and Finishing of Aluminum and Its Alloys* (ASM International, Metals Park, OH, 1987).
[12] G. E. Thompson and G. C. Wood, Anodic films on aluminum, *Treatise on mateirals science and technology*, Vol. 23, (Academic Press, New York, 1983).
[13] A. Huczko, Appl. Phys. A: Mater. Sci. Process. **70**, 365 (2000).
[14] J. Choi, Y. Luo, R. B. Wehrspohn, R. Hillebrand, J. Schilling, and U. Gosele, J. Appl. Phys. **94**, 4757 (2003).
[15] G. S. Cheng and M. Moskovits, Adv. Mater. (Weinheim, Ger.) **14**, 1567 (2002).
[16] G. Schmid, J. Mater. Chem. **12**, 1231 (2002).
[17] H. Asoh, K. Nishio, M. Nakao, T. Tamamura, and H. Masuda, J. Electrochem. Soc. **148**, B152 (2001).
[18] V. P. Parkhutik and V. I. Shershulsky, J. Phys. D **25**, 1258 (1992).
[19] J. E. Houser and K. R. Herbert, J. Electrochem. Soc. **153**, B566 (2006).
[20] S. K. Thamida and H. C. Chang, Chaos **12**, 240 (2002).
[21] V. V. Yuzhakov, H. C. Chang, and A. E. Miller, Phys. Rev. B **56**, 12608 (1997).
[22] M. Sheintuch and Y. Smagina, Physica D **226**, 95 (2007).
[23] W. Guo and D. Johnson, Phys. Rev. B **67**, 075411 (2003).
[24] F. Q. Yang, Electrochem. Solid-State Lett. **9**, C44 (2006).
[25] C. Sample and A. A. Golovin, Phys. Rev. E **74**, 041606 (2006).
[26] G. K. Singh, A. A. Golovin, I. S. Aranson, and V. M. Vinokur, Europhys. Lett. **70**, 836 (2005).
[27] G. K. Singh, A. A. Golovin, and I. S. Aranson, Phys. Rev. B **73**, 205422 (2006).
[28] A. L. Friedman, D. Brittain, and L. Menon, J. Chem. Phys. **127**, 154717 (2007).
[29] A. L. Friedman and L. Menon, J. Appl. Phys. **101**, 084310 (2007).
[30] Z. Wu, C. Richter, and L. Menon, J. Electrochem. Soc. **154**, E8 (2007).
[31] S. H. Park, Y. Lee, J. K. Lee, and K. B. Kim, Electrochem. Solid-State Lett. **9**, D31 (2006).
[32] J. W. Diggle, T. C. Downie, and C. W. Goulding, Chem. Rev. (Washington, D.C.) **69**, 365 (1969).
[33] J. W. Diggle, *Oxides and Anodic Films* (Marcel Dekker, New York, 1973), Vol. 2.
[34] A. J. Bard and L. R. Faulkner, *Electrochemical Methods* (Wiley, New York, 1980).
[35] M. Z. Bazant, K. Thornton, and A. Ajdari, Phys. Rev. E **70**, 021506 (2004).
[36] O. Stern, Z. Elektrochem. Angew. Phys. Chem. **30**, 508 (1924).
[37] J. O'M. Bockris and A. K. N. Reddy, *Modern Electrochemistry* (Plenum, New York, 1970).
[38] M. C. Cross and P. C. Hohenberg, Rev. Mod. Phys. **65**, 851 (1993).
[39] D. Walgraef, *Spatio-Temporal Pattern Formation with Examples from Physics, Chemistry and Materials Science* (Springer-Verlag, Berlin, 1997).
[40] G. Paolini, M. Masoero, F. Sacchi, and W. Paganell, J. Electrochem. Soc. **112**, 32 (1965).
[41] M. A. Amin, S. Frey, F. Ozanam, and J.-N. Chazalviel, Electrochim. Acta **53**, 4485 (2008).